NUCLEATION AND GROWTH OF SUPPORTED METAL CLUSTERS AT DEFECT SITES ON MgO AND NaCl (001) SURFACES: THE CASES OF Pd AND Ag

J. A. VENABLES[#], G. HAAS[§], H. BRUNE[§] and J.H. HARDING*
[#]Department of Physics and Astronomy, Arizona State University, Tempe AZ 85287-1504, and School of Chemistry, Physics and Environmental Science, University of Sussex, Brighton, UK.
[§]Institut de Physique Experimental, EPFL, CH 1015 Lausanne, Switzerland.
*Department of Physics and Astronomy, University College, Gower Street, London, UK.

ABSTRACT

Nucleation and growth of metal clusters at defect sites is discussed in terms of rate equation models, which are applied to the cases of Pd and Ag on MgO(001) and NaCl(001) surfaces. Pd/MgO has been studied experimentally by variable temperature atomic force microscopy (AFM). The island density of Pd on Ar-cleaved surfaces was determined in-situ by AFM for a wide range of deposition temperature and flux, and stays constant over a remarkably wide range of parameters; for a particular flux, this plateau extends from 200 K $\leq$ T $\leq$ 600 K, but at higher temperatures the density decreases. The range of energies for defect trapping, adsorption, surface diffusion and pair binding are deduced, and compared with earlier data for Ag on NaCl, and with recent calculations for these metals on both NaCl and MgO.

INTRODUCTION: NUCLEATION PROCESSES FOR METALS ON IONIC CRYSTALS

Thin metal clusters supported on oxide surfaces have many practical applications due to their catalytic, magnetic and electric properties. Many studies have therefore been performed on a range of model systems [1]. The main microscopic steps governing nucleation and growth of these films are now understood, yet a detailed characterization of these processes for metals on ionic crystals has proven difficult. The first studies of metal growth on alkali halide surfaces [2], and more recent studies on alkaline earth halides and oxides, have investigated defect nucleation based principally around transmission electron microscopy (TEM) [1,3]. On the other hand, a much more complete understanding has been achieved for the case of *metallic* substrates using variable temperature scanning tunneling microscopy (STM) for in-situ imaging of the nucleation and growth stages, compared to analytic models and numerical simulations [4]. Here we report a similar approach to metal growth on oxide surfaces using Atomic Force Microscopy (AFM) [5], showing that it can be used to determine the principal energies governing defect-influenced nucleation and growth for Pd deposited on MgO(001).

Nucleation on ionic oxide and halide surfaces are much more sensitive to defects than metals, such that defects can completely dominate the nucleation behavior. The rate equation treatment of nucleation and growth on perfect substrates has been extended to cover nucleation on random defect sites. A review of this work, with full historical references, was given for the 1996 MRS Fall meeting, and is also available in a recent book [6]. In recent years, quantum calculations of the binding of metal atoms and clusters to oxide and halide surfaces have progressed, generating further stimulus for experimental determination of the relevant interaction parameters, as a check of the reliability of the calculation methods. We report new calculations of the various energies needed to understand nucleation and growth for both Pd and Ag on MgO and NaCl, and comment on the level of agreement reached to date [7].

Mat. Res. Soc. Symp. Proc. Vol. 570 © 1999 Materials Research Society

EXPERIMENTAL PROCEDURES AND RESULTS

The growth of Pd on MgO(001) surfaces has been studied utilizing variable temperature atomic force microscopy (AFM) for imaging of the deposits [5]. This is one of the most explored metal/oxide systems, being a prototype model for supported metal catalysts. Pd grows in three-dimensional (3D) clusters, similar to most metal-oxide systems, as the surface energy is usually higher for metals than for oxides [1]. This thermodynamic argument may be overridden by kinetic effects, as apparently is the case for Ag/MgO [8]. In particular, it is well known that the preparation of the MgO surface has a pronounced influence on the structure of the deposits [1], and that more careful preparation may lead to 2D clusters and layers which are metastable [8]. Here we demonstrate for the Pd/MgO(001) system that the nucleation kinetics in a large temperature range is determined by attractive point defects. With the help of a simple rate equation model developed in the next section we deduce the relevant interaction energies.

The experiments were performed with a variable temperature atomic force microscope (AFM), mounted in a standard UHV chamber. The AFM, of the Besocke Beetle-type, utilizes piezoresistive cantilevers for force detection. This set-up allows easy tip exchange without breaking vacuum, and imaging of the MgO samples in the temperature range 100-500 K in contact and non-contact modes. MgO disks 2.7 mm thick and 23 mm in diameter were prepared by cleaving a single crystal rod along the (001) plane under Ar gas, and introduced into UHV by a load-lock without exposing them to ambient atmosphere. Heating and cooling was achieved by thermal contact to the sample holder, which could be electron beam heated and liquid nitrogen or helium cooled. The sample temperature was calibrated by a thermocouple glued to the center of a MgO sample before the experiments. Prior to deposition of Pd the crystal was heated in oxygen (10^{-4} mbar, 750 K, 30 min.).

AFM imaging of the surface revealed flat terraces 30-500 nm wide and typically several μm long, separated by mono- or multi-layer steps. Palladium was deposited from an electron beam heated Pd rod evaporator with a repelling voltage on an aperture between rod and sample to avoid ions reaching the surface. For the experiments presented here, a coverage of about 0.1 ML was deposited at a flux of 3.2×10^{-2} ML/min. (1ML = 1.13×10^{15} cm^{-2}). Auger electron spectra (AES) recorded after deposition revealed no change in sticking of Pd between 200 and 750 K, indicating complete condensation in that temperature range. Condensation was clearly incomplete at 800 K, where about ten times more Pd had to be evaporated onto the sample to get a similar Pd AES-signal.

The influence of the deposition parameters, substrate temperature and flux, were studied in detail. For each experiment, Pd was evaporated at a different substrate temperature onto a freshly cleaved MgO surface, and AFM images obtained in-situ after Pd deposition were recorded in non-contact mode, and shown in figure 1(b) and (c). Since these images represent a convolution of the island shape with the AFM tip, even for the low coverage deposited (0.1 ML) the surface seems largely covered at the lower temperatures. An estimation of the diameter of the islands from their height and density as well as the amount of Pd deposited gives a diameter of 1-2 nm (height ca. 0.4 nm) for 500 K and about 2-3 nm (height ca. 1.2 nm) for 745 K, considerably less than the apparent diameter in the images. Previous TEM experiments indicate epitaxial growth of Pd on MgO(001) and a truncated half octahedral or pyramidal shape, depending on growth conditions [1,3]. We chose to image the particles in the non-contact mode, since in contact mode (forces down to 10 nN) the small Pd particles were displaced by the tip to the borders of the scanned region.

The island density has been determined from AFM micrographs for a wide range of substrate temperature T and deposition flux F. The data points in figure 1 are an Arrhenius representation of the experimental island density N_x. The density stays constant over a remarkably wide span of temperatures, characteristic of nucleation at defects. The island density of the plateau is the number density of defects that act as traps for Pd ($\cong 3x10^{12}$ cm^{-2}). We are not able to identify the nature of these defects unambiguously for the moment, but the majority of the islands are not at steps, which can be readily observed by AFM. These additionally act as nucleation centers, as is seen for the three steps in the 500 K picture in figure 1(b) (diagonal lines). The typical island depletion zone around the steps is apparent in this image. But most of the islands are situated between the steps on the terrace; this is the density plotted on figure 1(a). Our preparation technique of cleaving under Ar clearly results in a *reproducible* density of such defects. Measurements with MgO samples cleaved *in-situ* in UHV gave a similar density.

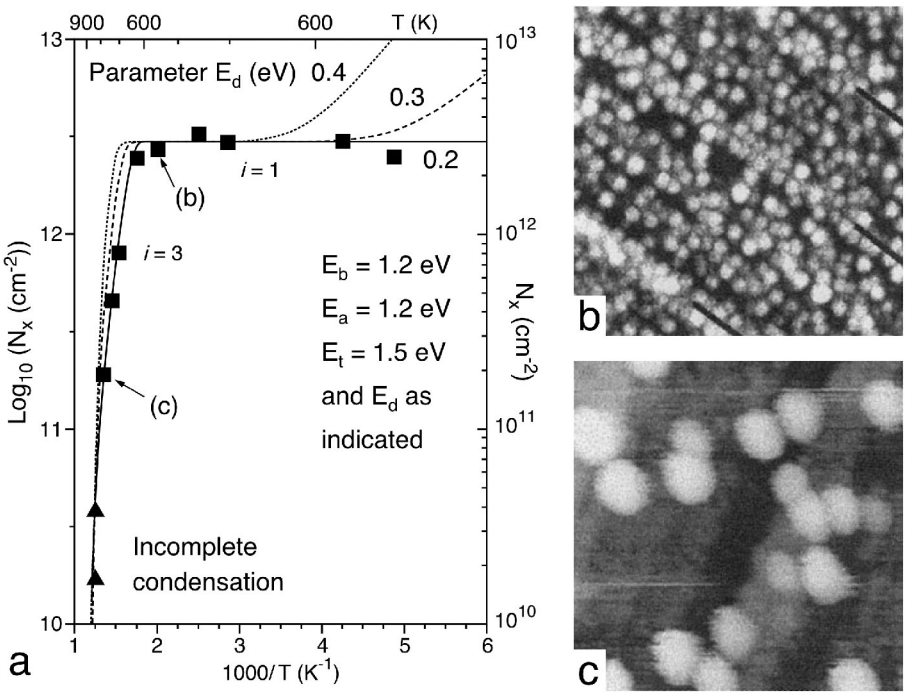

Fig. 1: a) Arrhenius representation of Pd island density N_x (cm^{-2}) at 0.1 ML coverage. The solid line is a "best fit" obtained with a rate equation model for $E_d = 0.2$, $E_t = 1.5$, $E_b = 1.2$ and $E_a = 1.2$ eV, plus curves for $E_d = 0.3$ (dashed) and 0.4 eV (dotted lines); b) and c) non-contact AFM images of Pd deposits on Ar-cleaved MgO(001). The substrate temperature during deposition was b) 500 K, with 3 lines indicating steps, c) 745 K. The size is 100x100 nm^2 for both images.

The influence of Pd flux F (or equivalently the deposition rate R) is as follows. In the plateau region (450 K) the island density was unchanged when the flux was varied over two decades. At high temperatures (745 K) the dependence is very weak. In a double logarithmic plot of N_x

versus F we find a slope of 0.07, well below the expected values between 2/7 and 1 for the case of homogeneous nucleation, depending on the size of the critical nucleus [9]. There are other examples in the literature where nucleation on surface point defects takes place [2,10], but the low flux dependence typically has not been checked explicitly. A recent example is furnished by high resolution UHV scanning electron microscope (SEM) observations of the growth of nm-sized Fe and Co particles on various CaF_2 surfaces, typically thin films on Si(111). In that work [10], the nucleation density, for a coverage of the surface by 3D islands $Z = Z_0 \cong 0.2$ close to the maximum density, was independent of temperature over the range 293-573 K. From the present results, we would expect a similar lack of flux dependence in this plateau region for these growth systems.

RATE EQUATION MODELS OF DEFECT-INFLUENCED NUCLEATION

In attempting to describe the nucleation and growth of thin films quantitatively, we need to include and then understand several parameters. The simplest defect-free surface model needs 3 activation energies: the adsorption energy E_a yields the adsorption stay time τ_a, and the diffusion energy E_d the diffusion constant D; the mean square diffusion distance before re-evaporation (without nucleation) is $D\tau_a$. The critical nucleus size, i, enters via the cluster binding energy E_i; in the simplest case this is related to the pair-binding energy E_b by bond counting [4,6,9].

Defects of various types can be incorporated into either analytical treatments or simulations, at the cost of at least two additional material parameters, the trap density n_t, and the trap energy E_t. Here we focus our attention on the rate equation for the nucleation density, and on the role of attractive surface point defects in promoting nucleation. We then estimate the magnitude of trapping energies by comparison with experiment, and enquire whether these values can be calculated reliably. We examine the simplest model, which presumes that just one type of trap is present, and that dimers and larger clusters can neither diffuse, nor leave the defect traps.

The nucleation density of islands on defective substrates can be derived by extending the equation for the maximum or saturation density of 2D islands of homogeneous nucleation [9]. This equation expresses the saturation density, n_x (to be compared with experimental density N_x) in combination with the coalescence expression $U_c = 2n_x dZ/dt$, as

$$n_x (g + r)^i (Z_0 + r) = f(F/D)^i \{\exp(E_i/kT)\}(\sigma_x D\tau_a)^{i+1}, \quad (1)$$

where the slowly varying numerical functions f and g involve the capture numbers σ_i and σ_x of critical and stable clusters respectively. For 3D islands, n_x is replaced by $n_x^{3/2}$ on the left hand side of (1), and the constants change a little. The critical nucleus size i and the regime of condensation (given by the ratio between surface residence and capture times of adatoms $r = \tau_a/\tau_c >$ or < 1) are both determined self-consistently as an output of an iterative calculation for given input adsorption, diffusion and binding energies (E_a, E_d and E_b).

Equation (1) has been shown to give correct parameter dependencies in the various limits [9]. The right hand side of this equation is proportional to the nucleation rate via the term in $\exp(E_i/kT)$, which is enhanced by a ratio $B_t = 1 + A_t$ with defects present [6]. To make this relationship clear, we start by considering the model of point defect traps shown in figure 2, constructing a suitable differential equation for the number of adatoms attached to traps, n_{1t},

$$dn_{1t}/dt = \sigma_{1t} D n_1 n_{te} - n_{1t} \nu_d \exp(-(E_t + E_d)/kT), \quad (2)$$

where n_{te} is the number of empty traps $= n_t - n_{1t} - n_{xt}$ and σ_{1t} the capture number of traps for adatoms.

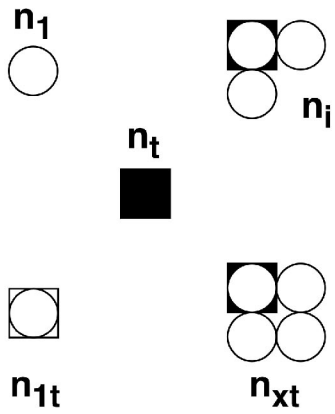

Fig. 2: Model for nucleation at randomly placed point defects with variables n_1: number density of free adatoms; n_t: density of traps; n_{1t}: density of trapped adatoms; n_i: density of critical clusters (shown for the case of $i = 3$, the critical cluster for the case $i = 1$ being a single adatom); n_{xt}: density of trapped stable clusters (clusters with atom numbers > i). The total density of stable clusters (trapped and free) is n_x. See text for discussion.

After a short time, dn_{1t}/dt reaches a steady state value of zero; inserting the usual expression for the diffusion constant $D = (\nu_d/4)\exp(-E_d/kT)$ in ML units, we deduce

$$n_{1t}/(n_t - n_{xt}) = A/(1+A), \text{ with } A = n_1 C_t \exp(E_t/kT), \tag{3}$$

where C_t is an entropic constant, which has been put equal to 1 in the illustrative calculations performed here. Equation (3) shows that the traps are full ($n_{1t} = n_t - n_{xt}$) in the strong trapping limit, whereas they depend exponentially on E_t/kT in the weak trapping limit, as expected. This is thus a Langmuir-type isotherm for the occupation of traps; the trapping time constant to reach this steady state is very short unless E_t is very large; but if E_t is large, then all the traps are full anyway.

The total nucleation rate is the sum of the nucleation rate on the terraces and at the defects. The nucleation rate equation becomes, without coalescence,

$$dn_x/dt = \sigma_i D n_1 n_i + \sigma_{it} D n_1 n_{it}, \tag{4}$$

where the second term is the nucleation rate on defects, and n_{it} is the density of critical clusters attached to defects, σ_{it} being the corresponding capture number. In the simplest case where the traps only act on the first atom which joins them, and entropic effects are ignored, we have

$$A_t = n_{1t}/n_1 = (n_t - n_{xt})A/[n_1(1+A)]. \tag{5}$$

A high value of A gives strong trapping, in which almost all the sites unoccupied by clusters will be occupied by adatoms; in the simplest model we assume that *clusters* cannot leave the traps.

This model results in the s-shaped curves shown in figure 1 for the whole temperature range studied, illustrated for $n_t = 2.65\text{x}10^{-3}$ ML, $E_t = 1.5$ eV, E_b and $E_a = 1.2$ eV, and E_d in the range 0.2-0.4 eV, with an assumed value of $\nu_d = 3$ THz, which is appropriate for bulk Pd, if not for Pd/MgO where it may well be lower. Comparison with the Pd/MgO experiments allows us to

deduce the following points: To reproduce the large extent in temperature of the plateau the trapping energy E_t has to be high, ≥ 1.2 eV, and the diffusion energy must be low, ≤ 0.2 eV. The reason why a low value of E_d is needed is so that the adatoms can migrate far enough at *low* temperatures to reach the defect sites. For weak trapping, the main effect would be caused by the reduced diffusion constant D due to the time adatoms spend at traps, yet this case is in disagreement with the extent of the plateau. Thus, with such a high value of E_t, something else eventually intervenes at *high* temperatures. This feature is explored using figure 3.

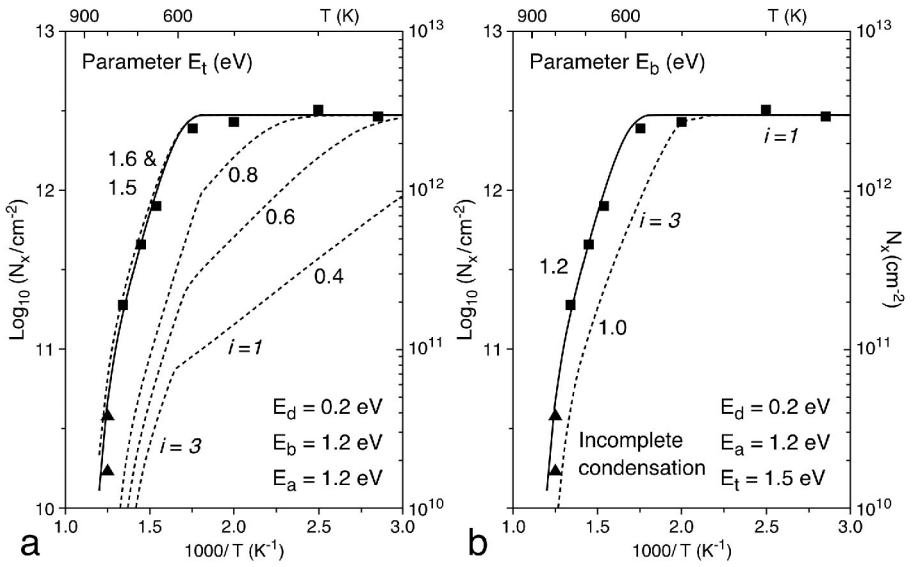

Fig. 3: a) Nucleation density predicted with trap density $n_t = 2.65\text{x}10^{-3}$ ML, $E_d = 0.2$ eV, E_a and $E_b = 1.2$ eV, and various values of trap energy E_t, as indicated; b) Nucleation density predicted with $n_t = 2.65\text{x}10^{-3}$ ML, $E_d = 0.2$ eV, $E_t = 1.5$ eV and $E_a = 1.2$ eV, for two values of the lateral pair binding energy $E_b = 1.0$ and 1.2 eV. The data points involving incomplete condensation are indicated by triangles, complete condensation by squares, as in figure 1a. See text for discussion.

There are two possibilities, given that an ad-dimer forms a stable nucleus at least up to $T \cong$ 600 K: one possibility is that condensation becomes incomplete at this point, but that ad-dimers remain stable, $i = 1$. This would indicate a lower limit to the value of E_b, with a moderate value of E_a being the important parameter. The other possibility is the inverse, where the first process to intervene is the transition to $i = 3$ (due to the square (001) geometry), i.e. the high temperature data determines E_b, and only at higher temperatures is the condensation incomplete. This means that the limiting process can become breakup of the cluster (on a trap), rather than removal of the adatom from the trap; E_t is not then itself important, provided it is high enough.

These two possibilities have different consequences for other measurements in the high temperature region; in particular the condensation coefficient is very different for the two cases. The observation of incomplete condensation via AES measurements, and the flux-dependent island density measurements are in agreement only with the second case. Figure 3 shows that $i =$

1 at low temperatures, but that the transition to $i = 3$ is responsible for the initial drop-off at high temperatures, followed by incomplete condensation at the requisite temperature to agree with observations. The plots with E_d = 0.2 eV correspond to our 'best fit', added in figure 1, indicating that both E_a and E_b are around 1.2 eV for Pd/MgO(001).

This model can be explored for other parameter values, but the fits are not as satisfying. If E_b is increased markedly (to 1.5 or even 2.0 eV) then the transition to i = 3 is delayed to higher temperatures; E_a then has to be reduced to fit the knee of the curve at 600 K, but now the higher temperature portion of the curve is much too steep, and incomplete condensation sets in too early. If E_b is reduced below about 1.0 eV the transition to $i = 3$ occurs too readily to fit the knee of the curve at 600 K, independent of the values of E_t or E_a.

CALCULATIONS OF RELEVANT ENERGIES

There are many schemes used to calculate interaction energies, which can then be used to relate the above experimental values to ab-initio theory. We have used classical atomistic simulation to calculate the energies E_a, E_d and E_b and defect parameters, which assumes that the interactions between atoms and ions can be described using a potential function; here we assume a central-force pair potential. There is a large number of such potentials available for MgO; we have used ref. [11]. The interactions between the ions and the atoms are obtained by calculation using the methods developed by Pyper and Wood [12]. The details of its application to Ag and Au on alkali halides are discussed in reference [7]. A basic outline follows.

First we calculate the interaction between the metal atoms and the ions within the Dirac-Fock approximation using suitable wavefunctions for the metal atoms and ions. It is important to calculate the oxide wavefunctions using a local potential to represent the effects of the lattice, because the O^{2-} ion is not stable in free space. Then estimates for the correlation and dispersion terms are added. The effects of metal polarizability are considered using a shell model. The polarizability of Ag is taken to be 60.73 a.u. from [13] and that of Pd to be 21.17 a.u. from the calculations of [14]. The interactions between the metal atoms in the dimer are fitted to a Morse potential. For silver, the data of [15] was used; for Pd the calculations of [16] were used. The resulting parameters are shown in the equations 6 and 7.

$$\text{For } Pd_2\text{: } V(r) = 1.220\ [\text{eV}]\ (1 - \exp(1.42018\ [\text{Å}^{-1}]\ (\ 2.4800\ [\text{Å}] - r\ ))) \quad (6)$$

$$\text{For } Ag_2\text{: } V(r) = 1.784\ [\text{eV}]\ (1 - \exp(1.43511\ [\text{Å}^{-1}]\ (\ 2.5303\ [\text{Å}] - r\ ))) \quad (7)$$

The surface structure was calculated using the MIDAS code [17]. This considers the crystal as a stack of planes divided into two regions. In the inner region (close to the interface) the ions are explicitly relaxed to positions of zero force. In the outer region, the block as a whole is permitted to move to allow for gross dilatation of the interface. The purpose of the outer region is to ensure that the forces on the outermost ions of the inner region are calculated correctly. The energies of the point defects are calculated using the CHAOS program [18]. The defects are created in the relaxed surface and the ions within an inner region (usually some hundreds of ions) are relaxed to positions of zero force. Ions outside this region are relaxed using the assumption of a dielectric continuum - the so-called Mott-Littleton approximation.

For the simpler configurations, some local density approximation (LDA) calculations are available [19, 20], and comparison with the present work is shown in Table I. The biggest discrepancy is for Pd over the Mg^{2+} site; however, the LDA calculations have a rather large basis-set superposition correction which reduces their accuracy. Overall the agreement is remarkably good, given that it is probably unreasonable to claim absolute accuracy < 0.1 eV.

Table I: Calculated adsorption energy of Pd and Ag on MgO (001)

Pd	(eV)	ref.[19] (eV)	Ag	(eV)	ref. [20] (eV)
Pd over O^{2-}	0.85	0.81	Ag over O^{2-}	0.66	0.66
over Mg^{2+}	0.24	0.59	over Mg^{2+}	0.22	0.36
over hollow	0.58	0.58	over hollow	0.56	0.53

We have calculated the behavior of monomers and dimers. This enables us to obtain the adsorption and migration parameters. These are shown in Table II.

Table II: Calculated adsorption and diffusion energies of monomers and dimers on MgO (001)

Pd	E_a(eV)	E_d (eV)	Ag	E_a(eV)	E_d (eV)
Monomer	0.85	0.2	Monomer	0.66	0.1
Dimer	1.47	0.3	Dimer	1.27	0.3

We have also considered trapping at surface defects. Duriez *et al.* [21] discuss the production of surface vacancies in the presence of water. The simplest possibility is a reaction of the form

$$O^{2-} \text{ (in surface)} + H_2O = 2\ OH^- \text{ (in surface)} + V(Mg^{2+}, \text{ in surface}) \quad (8)$$

where a magnesium ion vacancy is created because of the need to conserve lattice points. Pd binds to this Mg ion vacancy with an energy of 2.0 eV with respect to a Pd atom at infinity, i.e. the binding energy with respect to an atom already adsorbed on the surface is estimated to be 2.0 -0.85 = 1.15eV. The Pd atom sits within the vacant site but is too large to be drawn completely inside the MgO surface structure. This may be an alternative strongly binding defect to the oxygen atom vacancy on the O^{2-} site considered in reference [22].

COMPARISON WITH OTHER WORK

There are two types of comparison which can be made with other work, notably for Pd with experiments by the Henry group [1, 3, 21], and with ab-initio and other cluster calculations [19, 20, 22-24]. For Pd/MgO, recent density functional and other estimates of E_a gave 0.9-1.0 eV [19], with correction downwards to 0.81 eV [20, 23], encouraging us to believe our experimental value $\geq$ 1.0 eV. There are several literature estimates of the binding energy of the diatomic molecule Pd_2 in the gas phase, covering a huge range from 0.73 to 1.69 eV. However, empirical work and some recent calculations prefer the lower end of the range, with all calculations below 1.35 eV [24]. The value used here (equation 6) is 1.22 eV [16]. Given that values on surfaces are almost certainly less than free space values, $E_b \cong 1.2$ eV may well be quite reasonable.

The trapping energy of Pd in a surface oxygen atom vacancy has been estimated to be as high as 1.55 eV [22], provided the defect is a neutral F_s center, which has 2 electrons located between the vacancy and the Pd adatom. While this value cannot be regarded as definitive, it, plus the value of 1.15 eV calculated here for the Mg ion vacancy, indicates that high trapping energies can be envisaged, which are very specific to the chemistry of the particular metal adatom and to the charge state of the defect. For example, in ref. [22], the Ag adatom was found to be unbound to the F_s center, essentially because the second electron could not be accommodated on the Ag, so that the complex split into an F_s+ center plus an Ag+ ad-ion. This is real cluster chemistry, depending on the d^{10} (admixed with d^9s^1) state of Pd, versus $d^{10}s^1$ for Ag.

The island densities and the values for E_a, and in particular for (E_a-E_d) that we have deduced are considerably higher than those deduced from a series of experiments by the Henry group [1,3]. While we cannot at this stage uniquely identify all the causes of these differences, we note that if one has to invoke a spectrum of defect energies in order to explain a continuous variation of n_x with temperature, then the model contains too many parameters (either explicit or implied) to achieve a unique answer. What is clear from the experiments reported here is that our sample preparation technique produces a high density of one type of defect, which has a very high trapping energy for Pd adatoms. Under these circumstances the interpretation is clear, provided one remains within the simplest model that explains the results. It is encouraging that the energies needed are close to those resulting from state of the art cluster calculations.

Finally we can make comparisons with other related systems such as Ag/MgO, and with Pd, Ag and Au/NaCl, where some experimental and theoretical work has been performed. This will be the subject of further work, but meanwhile we can see that such comparisons should be fruitful from experimental, modeling and theoretical viewpoints. Calculated, and some experimental values of (E_a - E_d) are presented in Table III; this is the energy which determines the surface diffusion length before desorption in the absence of nucleation [2, 4, 9]. From the present calculations in particular, the dimer diffusion energy is often quite small, and this process has not usually been explicitly included into the rate equation modeling. This is despite the fact that it is known to produce characteristic effects, such as saturation of the nucleation density at low coverage. Calculated adsorption energies seem to be systematically low, by up to 0.2 eV, in comparison with experiment, and it may be that the (partial) charge transfer from the metal adatom to the ionic substrate is being underestimated. These are points to explore in future, subject, as always, to not introducing so many parameters that all fits are possible but nothing can be deduced. Calculations are now clearly important in guiding us as to which processes need to be considered. The strong trapping, and low diffusion, energies mean that one can envisage creating self-organized arrays of clusters based on nucleation at deliberately introduced defects.

Table III: Some comparisons of (E_a - E_d) [eV] for Pd, Ag and Au on MgO and NaCl substrates. Calculations from this paper and ref [7]. Experimental values in square brackets from the present work for Pd/MgO and from reviews [2, 4, 9].

	Pd /MgO	Ag/MgO	Pd/NaCl	Ag/NaCl	Au/NaCl
Monomer	0.65 [0.8-1.0]	0.56	0.40 [0.45]	0.12 [0.22]	0.08 [0.33±0.02]
Dimer	1.27	0.97		0.44	0.27

CONCLUSIONS

The present study demonstrates that a detailed understanding of the interaction of metals with oxide surfaces can be obtained by AFM experiment combined with a rate equation analysis containing the effects of attractive surface point defects. The observed trapping and nucleation of Pd clusters on MgO (001) is interesting from a fundamental point of view, but may also be of interest for producing novel supported nanostructures. Now that calculations of the relevant energies at oxide and halide surfaces are becoming reliable, there is also scope for detailed comparison of a number of related metal/oxide and metal/halide systems.

Acknowledgments: JAV is grateful to the conference organizers for their support, and to several colleagues for preprints and comments. JAV, GH and HB acknowledge work performed in conjunction with A. Menck, J. V. Barth and K. Kern which will be published more fully in

reference [5]. JAV and JHH acknowledge work performed in conjunction with A.M. Stoneham, some of which is published in reference [7]; the remainder is work in progress. #Corresponding author e-mail: john.venables@asu.edu

References: 1. C.T. Campbell, Surface Sci. Rep. **27,** 1 (1997); C.R. Henry, *ibid* **31**, 231 (1998).
2. M. Harsdorff, Thin Solid Films **90**, 1 (1982); *ibid* **116**, 55 (1984); J.L. Robins, Appl. Surf. Sci. **33/34**, 379 (1988); A.D. Gates and J.L. Robins, Surf. Sci. **191**, 499 (1987).
3. C. Chapon, C.R. Henry and A. Chenam, Surface Sci. **162,** 747; M. Meunier and C.R. Henry, *ibid* **307-309**, 514 (1994); C.R. Henry and M. Meunier, Vacuum **50**, 157 (1998).
4. H. Brune, H. Röder, C. Baragno and K. Kern, Phys. Rev. Lett. **73**, 1955 (1994); H. Brune, Surface Sci. Rep. **31**, 121 (1998); see also chapters by Venables, Brune and Kern in *Growth and properties of ultrathin epitaxial layers*, edited by D.A. King and D.P. Woodruff (The chemical physics of solid surfaces and heterogeneous catalysis vol **8,** Elsevier, 1997).
5. G. Haas, A. Menck, H. Brune, J.V. Barth, J.A. Venables, and K. Kern (1999) submitted for publication.
6. J.A. Venables, Mater. Res. Soc. Proc. **440**, 129 (1997); Physica **A239**, 35 (1997); Chapter 1 of *Heteroepitaxy: thin film systems*, edited by W.K. Liu and M.B. Santos (World Scientific, 1999).
7. J.H. Harding, A.M. Stoneham and J.A. Venables, Phys. Rev. **B57,** 6715 (1998) and to be published.
8. F. Didier and J. Jupille, Surface Sci. **307-309,** 587 (1994); A.M. Flank, R. Delauney, P. Lagarde, M. Pompa and J. Jupille, Phys. Rev. **B53,** R1737 (1996).
9. J.A. Venables, Phil. Mag. **27**, 697 (1973); Phys. Rev. **B36**, 4153 (1987); for a review see Surface Sci. **299/300**, 798 (1994) or refs 4.
10. K.R. Heim, S.T.Coyle, G.G. Hembree, J.A. Venables and M.R. Scheinfein, J. Appl. Phys. **80**, 1161 (1996).
11. M.J.L. Sangster and A.M. Stoneham, Philos. Mag. **B43,** 597 (1981).
12. N.C. Pyper and C.P. Wood, Philos. Trans. Roy. Soc. **A320,** 71 (1986).
13. A.A. Radzig and B.M. Smirnov, *Reference Data on Atoms, Molecules and Ions* (Springer-Verlag, 1985).
14. W.R. Johnson, D. Kolb and K.N. Huang, Atomic Data and Nuclear Data Tables **28,** 333 (1983).
15. V. Beute, H.G. Kramer, M. Kuhn, W. Weyers and W. Demtroides, J. Chem. Phys. **98**, 2699 (1993).
16. K. Balasubramanian, J. Chem. Phys. **89,** 6310 (1988).
17. P.W. Tasker, Philos. Mag. **A39,** 119 (1979).
18. P.W. Tasker and D.M. Duffy, Report No. AERE-11059 (1983).
19. I.V. Yudanov, S. Vent, G. Pacchioni, K. Neyman and N. Rösch, Chem. Phys. Lett. **275**, 245 (1997); K.M. Neyman, S. Vent, G. Pacchioni and N. Rösch, Nuovo Cimento **19D**, 1743 (1997);
20. L. Spiess, Surface Rev. Lett. **3,** 1365 (1996).
21. C. Duriez, C. Chapon, C.R. Henry and J.M. Rickard, Surf. Sci. **230**, 123 (1990).
22. A.M. Ferrari and G. Pacchioni, J. Phys. Chem. **100**, 9032 (1996).
23. A. Stirling, I. Gunji, A. Endou, Y. Oumi, M. Kubo and A. Miyamoto, J. Chem. Soc. Faraday Transactions **93**, 1175 (1997); N. López and F. Illas, J. Phys. Chem. B **102**, 1430 (1998).
24. I. Shim and K.A. Gingerich, J. Chem. Phys. **80**, 5107 (1984); M.D. Morse, Chem. Rev. **86,** 1049 (1986); M. Harada and H. Dexpert, J. Phys. Chem. **100**, 565 (1996); G. Valerio and H. Toulhoat, J. Phys. Chem. **100**, 10827 (1996); J.M. Seminario, A.G. Zacarías and M. Castro, Int. J. Quant. Chem. **61**, 515 (1997).